

2001-GT-0197

ON THE IMPACT OF BLADE COUNT REDUCTION ON AERODYNAMIC PERFORMANCE AND LOSS GENERATION IN A THREE-STAGE LP TURBINE

Jochen Gier and Sabine Ardey
MTU Aero Engines
D-80995 München
Germany

ABSTRACT

Reducing the number of blades in low pressure turbines is a desirable option for decreasing total operation costs. From an aerodynamical point of view this directly leads to an increased blade load. However, increasing the blade load above a certain level results in viscous effects like separation bubbles and finally full separation. This becomes especially significant for aero engine turbines, which operate at high altitudes and thus low Reynolds numbers. The underlying local flow phenomena and the effect on the aerodynamic performance of such configurations are addressed in this paper.

This investigation is based on a three-stage low pressure turbine typical for aero engines. Different setups are employed with different number of guide vanes in certain stages. Furthermore, the Reynolds number is varied within a wide range. These configurations are investigated numerically using a modern steady-state transitional Navier-Stokes solver and experimental results from the same turbine. Based on this information, a detailed analysis of the viscous flow phenomena is performed with focus on the influence of separation bubbles on the loss production after the transition. These results are discussed with respect to blade count reduction

NOMENCLATURE

| | | |
|-----------------|-------------------|--------------------|
| A | [m ²] | cross-section area |
| C | [-] | constant |
| <i>f</i> | [-] | function |
| H ₁₂ | [-] | form parameter |

| | | |
|------------------|-----------------------------------|---|
| k | [m ² /s ²] | turbulent kinetic energy |
| l | [m] | length |
| Ma | [-] | Mach number |
| n | [-] | factor |
| P | [W] | power |
| R | [J/kg K] | gas constant |
| R, Re | [-] | Reynolds number |
| Tu | [-] | turbulence intensity |
| u | [m/s] | velocity |
| x | [m] | coordinate length |
| y | [m] | wall distance |
| β | [-] | exponent |
| δ ₂ | [m] | boundary layer momentum thickness |
| φ | [W/m ³] | power of dissipative forces |
| μ | [Pa s] | dynamic viscosity |
| μ _{eff} | [Pa s] | μ _{laminar} + μ _{turbulent} |
| ν | [m ² /s] | kinematic viscosity |
| ρ | [kg/m ³] | density |
| ω | [1/s] | specific turbulence dissipation |
| ζ _v | [-] | total pressure loss coefficient = (p _{t2} - p _{t1})/(p _{t2} - p ₂) |
| Φ | [-] | loss production coefficient |

Subscripts

| | |
|------|-----------------------|
| i, j | indices of components |
| l | laminar |
| t | turbulent |
| w | wall |

INTRODUCTION

In the design of modern aero engines low total operating cost is one of the main targets. On the part of turbine components this leads to the reduction of the number of turbine blades in a row to reduce production and maintenance cost. But this increases the airfoil load and thus has a possibly negative impact on the aerodynamic performance. Especially in engines for business jets, cruising at high altitudes, maintaining a high efficiency level becomes even more difficult with increasing blade load.

The reason is that at high flight levels the ambient pressure drops significantly and so does the Reynolds number of the flow. Decreasing the Reynolds number of the flow while pushing up the blade load increases the danger of flow separation on the suction side of the airfoil. At typical cruise conditions the LPT airfoils are usually designed to have laminar flow along some parts of the suction surface and turbulent conditions in the rear part after going through a laminar-turbulent transition. Often there is a small separation bubble inside the boundary layer, where the flow reattaches after the transition sets on.

There are quite many publications dealing with the development of boundary layers and separation bubbles in low-pressure turbines. Stratford, 1957, investigated laminar separation phenomena in boundary layers. Tan and Auld, 1991, performed hot wire tests on a turbine cascade in a low speed wind tunnel at various Reynolds numbers with transition and separation bubbles. In their paper they reported the variation of different boundary layer parameters.

Schröder, 1991, showed very extensive experimental investigations with special focus on unsteady hot-film measurements of the boundary layer flow in a five-stage low-pressure turbine. The paper focussed on the interaction of turbulence, transition and blade row passing. Similar investigations were made in a LPT cascade with simulated incoming wakes by Engber and Fottner, 1995. More experimental data on the flow and turbulence quantities in separated boundary layers with reattachment and transition were performed e.g. by Rivir, 1996, Qui and Simon, 1997, Sohn et al, 1998 and Hatman and Wang, 1998a, 1998b, who conducted experiments on separated flow transition and used this data to develop a model for transition in these flows.

Today numerical solutions of the Navier-Sokes equations have become a commonly used tool in the development of turbines, e.g. Scrivener et al, 1991. For the prediction of separation bubbles and transition an adequate turbulence and transition modelling has to be applied. Since popular turbulence models like the algebraic Baldwin-Lomax model, 1978, or many variants of linear two-equation models are not capable or not reliable enough to accurately predict transition, transition is usually modelled separately. An accurate transition prediction is essential for the computation of separation bubbles.

Frequently used transition models are the ones based on Mayle, 1991, Abu-Ghannam and Shaw (AGS), 1980 and Roberts, 1980. Among these the AGS-model is well established and has been chosen for this investigation in a modified version. Comparison of different transition models and their application to low-pressure turbine flows are reported e.g. by Sanz and Platzer, 1996 and Chernobrovkin and Lakshminarayana, 1999, who even took a close look into the influence of the numerical scheme on the transition prediction. Dorney et al, 1999 carried out an investigation of unsteady flow and transition phenomena at mid channel height of a two-stage low-pressure turbine.

Some new aspects in predicting bypass transition were presented by Mayle and Schulz, 1996.

However, there is very little literature published with respect to the losses connected with the appearance of separation bubbles on the suction surfaces of LP turbines. Scrivener et al, 1991, give some loss information downstream of the blade row. Denton, 1993, provides a very comprehensive overview over loss mechanisms in turbomachines with special emphasis on the concept of entropy generation. He gives a good classification of the different types of losses encountered in turbomachinery.

To the knowledge of the authors there is no investigation reported in literature, which takes a close look not only into the flow and turbulence structure of separation bubbles with transition but also into the loss generation in these flows. Therefore, this paper addresses the loss generation in boundary layer separation bubbles in connection with transition by applying a Navier-Stokes code with transition model to a three-stage low-pressure turbine.

This methodology is employed to assess the loss production process along the suction side boundary layer and some major influences in turbines, the flow Reynolds number and the airfoil load.

EXPERIMENTAL SET-UP

The three-stage test turbine was installed at the high altitude test facility at the University of Stuttgart, Germany. The test rig can be operated in a mode with a closed gas circuit in order to run the rig at Reynolds-numbers typical for jet engines with separately adjustable inlet and exit conditions.

In figure 1 a cross section of the test turbine is shown. To assess reliable inflow conditions pressure and temperature are measured in several radial and circumferential positions. In the exit plane pressure and temperature probes with 10 radial measuring locations are installed. Additionally a traversable 5-hole probe was used to measure data for static pressure, total pressure, Mach-number and flow angles. The entire outflow measuring installation can be traversed circumferentially by 2 pitches of vane 3. Furthermore vanes 1, 2 and 3 are instrumented with pressure taps for wall pressure in 3 radial positions. Efficiency is determined on the basis of temperature measurements.

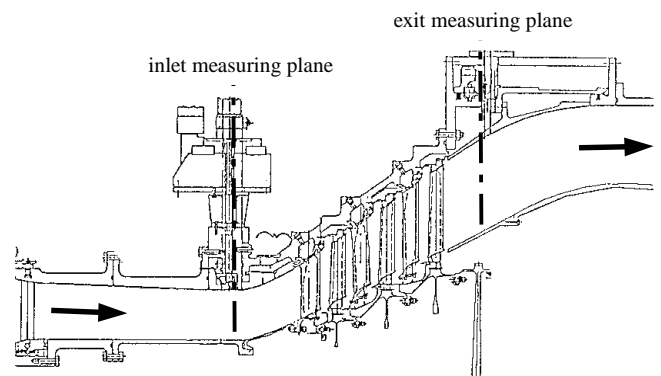


Figure 1: Cross sectional view of test rig

Upon completion of the experiments the boundary layer flow was visualised with a colour injection into to inflow. The injection was done for the reference Reynolds-number case ($Re = 300,000$).

NUMERICAL METHOD

The simulations are performed with the TRACE_S 3D compressible Navier-Stokes code, which is based on a block-structured finite volume scheme. The code computes the multiple rows fully coupled. Time integration is done using an explicit Runge-Kutta procedure in combination with implicit residual smoothing and local time stepping. Central differencing is employed for the convective fluxes with artificial 2nd and 4th order damping according to Swanson and Turkel, 1987. In order to provide stable solutions even in very complex flows, without introducing too much damping elsewhere, a special sensor for 2nd and 4th order blending was used.

The stage coupling is based on the mixing plane technique with no-reflecting boundary interfaces, flux averaging and full mass conservation. For reduction of computation and turnover times the code is vectorised and able to use shared memory parallelisation (SMP) as well as distributed memory parallelisation. More information about the numerical details can be found in Fritsch et al, 1997.

Turbulence Modelling

Since this investigation intends to take a close look into the transitional boundary layers in a LP turbine, a sufficiently fine mesh resolution of the profile boundary layers is necessary. Therefore, the Wilcox $k-\omega$ two-equation model in low-Reynolds version was employed with extensions for compressibility and system rotation (Wilcox, 1988).

The equations are time-discretised by 2 x 2 block-implicit time stepping. The resulting system of equations is solved with a red-black Gauss-Seidel iteration technique. For more details please also refer to Gier et al., 2000.

Transition Modelling

In principle low-Re two-equation turbulence models are capable of simulating by-pass transition. However, not only a sufficient grid clustering perpendicular to the wall but also sufficient grid density in streamwise direction is needed to obtain good results. In multistage turbines the usually high free-stream turbulence level inside the passage in combination with favourable and adverse pressure gradients is further impairing a reliable transition prediction.

Therefore a transition model is employed in combination with the $k-\omega$ turbulence model in this investigation. It is based on the correlations of Abu-Ghannam and Shaw, 1980 with modifications of Drela, 1995. The choice among the variety of different models fell on this model, because it takes the boundary layer shape and thus the pressure gradients into account. It is also dependent on the free-stream turbulence level, which is taken from the local turbulence level at the boundary layer edge provided by the turbulence model.

The model affects the turbulent viscosity and thus also the turbulence production. The starting point for transition is set, where the Reynolds-number parameter R_{Θ_s} exceeds the threshold value R_{δ_2} .

$$R_{\Theta_s} = 163 + C_{11} [C_{12} \cdot f(H_{12}) + 1] \cdot (C_{1T} \cdot n_{crit} + 1) \quad (1)$$

$$H_{12} = \delta_1 / \delta_2 \quad (2)$$

$$n_{crit} = C_m - 2.4 \cdot \ln(Tu) \quad (3)$$

$$R_{\delta_2} = \frac{u_\infty \delta_2}{\nu} \quad (4)$$

The quantities C_{ti} are constants. This criterion is combined with an intermittency function f_i , which takes values between 0 and 1 to model the growth process of the turbulence.

$$f_i = \left[\frac{25}{25 + 275 \cdot \left(1 - \sin \left(\frac{\pi}{2} \cdot \frac{R_{\delta_2} - R_{\Theta_s}}{R_{\Theta_s}} \right) \right)} \right]^\beta \quad (5)$$

with $\beta = 3$

The transition model is applied to the entire suction surface except the leading and trailing edge, where the data of Abu-Ghannam and Shaw is not applicable, because it was gained in flat plate experiments. Due to the steady-state assumption of the computation the unsteadiness of the turbulence is averaged out in the steady-state values of turbulent energy k and dissipation ω .

Boundary Conditions and Computational Mesh

Non-reflecting boundary conditions are applied at inlet and outlet. Distributions of the measured total pressure, total temperature and flow angle distributions are prescribed at the inlet and static pressure at the outlet. The inlet turbulence intensity is 1% which is lower than in a real engine because of the specific test rig configuration.

At solid walls velocities are set to zero except for rotating walls. All walls are assumed to be adiabatic. Turbulent kinetic energy is set to zero and the specific dissipation rate ω is determined according to:

$$\omega_w = \frac{6\mu_w}{(C_{\epsilon 2} - 1) \cdot C_\mu \rho y_w^2} \quad (6)$$

At the endwalls, where the cavities are neglected, a fully turbulent flow regime is to be expected. Therefore, a wall function according to Spalding, 1972 is employed there, enabling the use of a coarser endwall grid resolution without a significant loss in accuracy and thus reducing the computational effort significantly.

The computational mesh consists of 12 blocks. Each vane or blade is gridded with one O-type grid around the airfoil and a H-type grid for the major part of the channel. For resolving small flow features and to assure a dimensionless wall distance y^+ towards the profiles of about 1 the boundary layer grid is heavily clustered close to the surface. The resulting number of grid nodes in a row is approximately 700,000 with 65 nodes in radial and effectively 97 nodes in circumferential direction. The total number of grid nodes is about 4.3 million. This grid structure and resolution is currently used for high-end design applications with turnaround times of less than 10 hours on a NEC SX4 vectorcomputer in parallel mode. Some of the underlying computations have been performed on a cluster of SGI Octane workstations using the MPI version of the code. All results were accepted as converged, when massflow and efficiency of the component and the individual stages remained constant with residuals down by at least 2 orders of magnitude.

FLOW CHARACTERISTICS OF THE TEST TURBINE

As mentioned above the investigated test turbine is a three-stage low pressure turbine typical for aero engine applications. The aspect ratio of the blade rows is on today's standard high level. The blade rows have a conventional number of airfoils except vane 2, where the airfoil number is reduced from 138 (original design, case V2_138) to 111 (-20 %, case V2_111) thus increasing the aspect ratio beyond accepted design limits.

In the underlying experiments three Reynolds numbers have been investigated. The intermediate Reynolds number of 300,000 is close to the design point of operation and will be used as reference. The other two Reynolds numbers are approximately twice and half of the reference value (table 1). The Reynolds numbers are based on the flow status downstream of vane 1 and the axial chord length of vane 1.

| Reynolds number | 140,000 | 300,000 | 550,000 |
|-----------------|---------|---------|---------|
| abbreviation | Re140 | Re300 | Re550 |

Table 1: Investigated Reynolds numbers based on vane 1

The airfoils have a typical low pressure turbine design with an aft-loaded pressure distribution. Thus, there are no significant flow separation effects present on the pressure surfaces. The suction surfaces are designed in a way, that small separation bubbles with reattachment occur at the reference Reynolds number. Upstream of these separation bubbles the flow within the suction side boundary layer is laminar. The bubbles then trigger the laminar-to-turbulent flow transition, which sets in across the bubble. Downstream of the separation the flow becomes fully turbulent, reattaches again and develops a turbulent boundary layer.

In order to compute realistic flow structures for these bladings, especially when losses are addressed, the flow solver has to be able to capture the transition. The insufficiency of a fully turbulent calculation where transition is omitted were shown by Gier et al. 2000. Therefore, the above mentioned transition modelling was employed for all computations in this paper.

In figure 2 the surface pressure distribution of the 2nd vane is plotted. It is obvious that the aerodynamic load is higher in the case V2_111. This is the result of reducing the airfoil count, while trying to preserve the turning and acceleration of the vane. In both cases there is a little bump on the suction side indicating a separation bubble with reattachment. Due to the different airfoil shape this bubble is detected further downstream in the V2_138 case. Computation and experiment correspond quite well. Only the minimum pressure is slightly overpredicted, which can at least partly be attributed to the tolerances in the pitch of the test turbine.

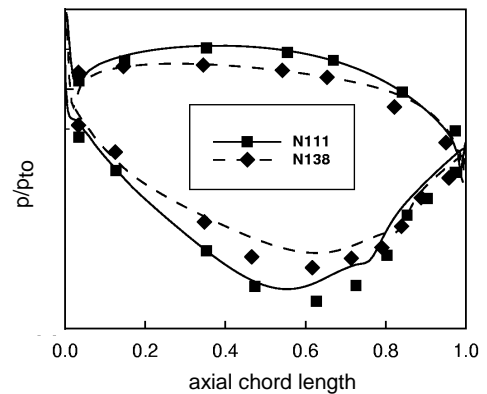


Figure 2: Surface pressure distribution of 2nd vane, comparison of cases V2_111 and V2_138 cases, Re = 300,000

A variation of the Reynolds-number has some significant impact on the flow pattern of the bladings and consequently also on the efficiency. In the following it will be presented for the more ambitious low blade count case (V2_111). On the suction side of vane 1 a turbulator had been installed in the experiments to trigger an early transition to turbulent flow. This was done to model the influence of a higher inlet turbulence level caused by an upstream high pressure turbine present in an actual aero engine and thus to impair a flow separation. In terms of the computation this was modelled by turning off the transition model for this vane. The result is a well matched pressure distribution for all Reynolds numbers.

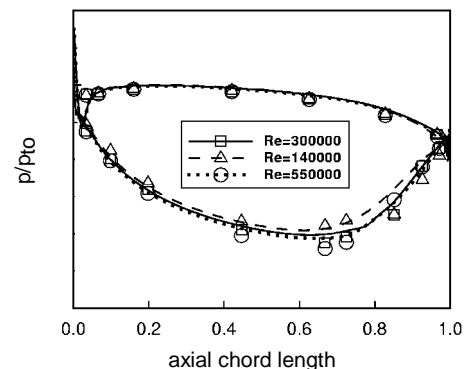


Figure 3: Surface pressure distribution of 1st vane, comparison of different Reynolds numbers (V2_111)

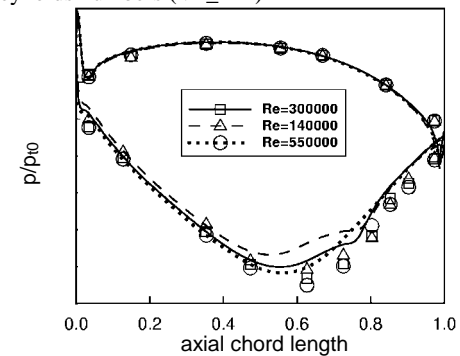


Figure 4: Surface pressure distribution of 2nd vane, comparison of different Reynolds numbers (V2_111)

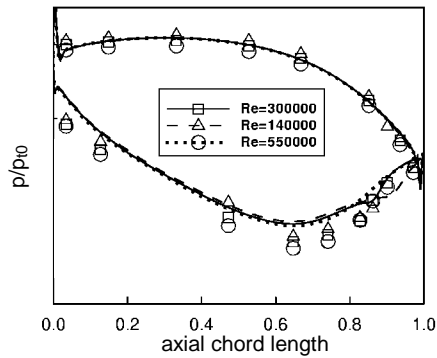


Figure 5: Surface pressure distribution of 3rd vane, comparison of different Reynolds numbers (V2_111)

In vanes 2 and 3 (fig. 4 and 5) the use of the transition model leads to the detection of separation bubbles for the two lower Reynolds number cases. At $Re = 550,000$ there is no separation bubble present as expected. The simulation corresponds quite well with experimental data for all Reynolds numbers. As mentioned above, the slight overestimation of the minimum pressure on the suction side can be at least partly put down to deviations of the pitch in the experimental set-up.

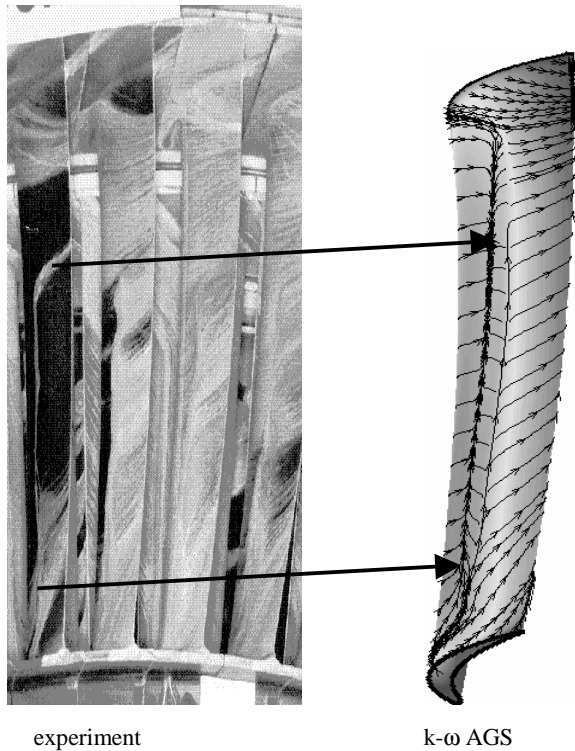


Figure 6: Streamtraces on suction surface of 2nd vane (V2_111), view from downstream, $Re = 300,000$

For the intermediate Reynolds number the near-wall flow was visualised by colour injection. Figure 6 shows the resulting streamtraces on the suction side of vane 2 in comparison with numerical results. For the numerical results, the flow direction was taken from the flow in the 1st cell layer of the numerical grid. It can be seen that a flow separation with reattachment is present. The extend

and position of the bubble in streamwise direction is very well matched. Also the extend and direction of the secondary flow features close to the side walls connected to the passage vortices correspond well in computation and experiment. Only the radial extend of the separation bubble close to the casing is somewhat overpredicted for two possible reasons: In some situations the transition model may predict transition a little bit too late and/or the influences due to the casing cavity flows are not accounted for in this simulation

The resulting radial efficiency is plotted in figure 7 for the V2_111 case. Numerical and experimental results show the same trends and correspond quite well with each other for all Reynolds numbers.

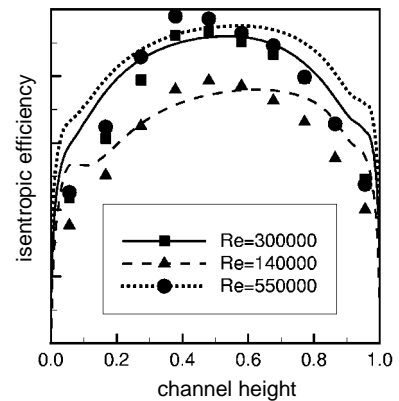


Figure 7: Isentropic efficiency of test turbine, comparison of different Reynolds numbers, experiment and numerical solution

The efficiency is overpredicted in the regions close to hub and casing. This can not be attributed to any deficiency of the transition model. All the more so, because the Wilcox $k-\omega$ model is well suited for 3D flows, since it does not use any wall distance functions. The authors attribute this phenomenon to neglecting the cavity flows across the clearance seals in the current computations. Cavity flows insert low energy fluid in the endwall region of the turbine and may also create a shift of the next blade's angle of attack. This incidence then can also cause increased profile losses.

LOSS GENERATION WITHIN THE BOUNDARY LAYER

As seen above, the numerical simulation captures the boundary layer flow features including the separation bubble on the suction sides. For the following analysis the second guide vane is chosen from the three turbine stages, since it is located inside the component and is thus not subject to special effects of the inflow. Furthermore, the two different airfoil count numbers of the second guide vane offer the chance to observe the boundary layer behaviour under different load conditions.

First of all a measure of the losses encountered in the turbine has to be found and defined. For this investigation a loss parameter has to be chosen, which enables the comparison of loss generation for the different investigated Reynolds numbers. Changing the Reynolds number means that the pressure level changes and thus the massflow and power output. The authors felt that just looking onto total pressure loss or entropy of the entire blading would not be sufficient to locate

the local rate of loss production and this would also ignore the information to be gained from the flow solution.

Therefore, the specific power of the frictional forces as computed by the Navier-Stokes code is used as a measure for the loss generation quantity. This represents the rate of conversion of kinetic and potential energy into thermal energy. Thus it can stand for the rate of entropy generation.

$$\phi = \mu_{eff} \cdot \left\{ 2 \cdot \left(\frac{\partial u_i}{\partial x_i} \right)^2 - \frac{2}{3} \left(\frac{\partial u_i}{\partial x_i} \right)^2 + \left(\frac{\partial u_i}{\partial x_j} + \frac{\partial u_j}{\partial x_i} \right)^2 \right\} \quad (7)$$

In order to make a reasonable comparison between the different Reynolds numbers, this quantity is non-dimensionalised by a specific power of the respective turbine stage:

$$\Phi = \frac{\phi}{\phi_{ref}} = \frac{\phi}{\left(\frac{P_{stage}}{A_{cross-section} \cdot l_{stage}} \right)} \quad (8)$$

The local rate of loss production in the numerator of this function is referenced by an average power density of the turbine stage, which is defined as the stage power divided by an approximated volume of the stage. Hence, Φ -values of the order of one or more mean, that the local loss generation is stronger than the average power density, indicating a high loss production region. If Φ is far below one, the flow is basically inviscid.

In figure 8 the Φ -distribution is shown for the vane 2 with the higher load (V2_111) at a Reynolds number of 300,000.

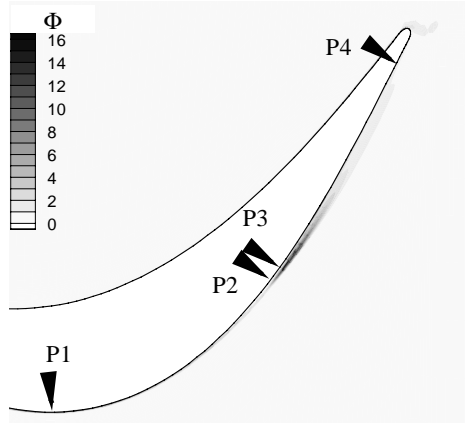


Figure 8: Distribution of Φ in vane 2 (V2_111), mid-span, $Re=300,000$

There are basically three regions, where increased loss occurs: the thin shear layer at the wall, the wake and the region of the separation bubble close to position P3. The rest of the flow shows Φ -value magnitudes below one.

In position P1 the flow inside the boundary layer is laminar as predicted by the transition model. This can be seen in figure 9 (P1), where the distributions of Φ , μ_{eff}/μ_t and Ma in the boundary layer region are plotted against the wall distance. Since the boundary layer is laminar, μ_{eff}/μ_t equals 1 close to the wall. The loss distribution has

its maximum at the wall, where the shear is the largest. At the boundary layer edge, Φ approaches zero in absence of any significant velocity gradients. The boundary layer thickness at this position with still accelerating flow is relatively thin.

At position P4 (fig. 9) a little upstream of the trailing edge, the boundary layer has become fully turbulent after it has reattached downstream of the separation bubble (positions P2 and P3). Within the displayed wall distance the boundary layer edge is not reached, because the boundary layer has grown quite considerably in the decelerating flow regime. The turbulent viscosity shows a steady increase from 1 at the wall (laminar sublayer) to a maximum at a distance of about 0.8 mm from the wall. Like in position P1 the maximum loss peak is located in the high shear region close to the wall. The peak value, however, is only about one third compared to P1, because in this decelerated flow the wall velocity gradient is smaller at basically the same molecular viscosity.

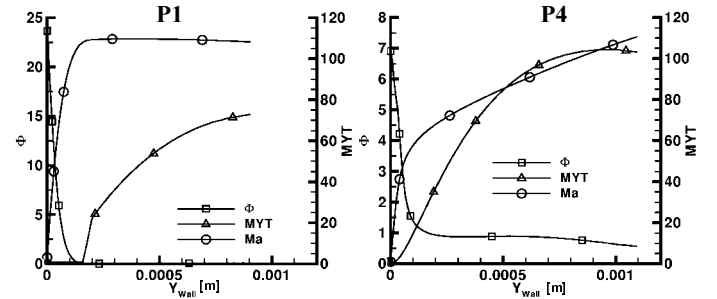


Figure 9: Distribution of Φ , μ_{sum}/μ_t (MYT) and Ma close to the wall in vane 2 (V2_111), mid-span, $Re=300,000$ at position P1 and P4

At about 0.1 mm wall distance the turbulent viscosity, i.e. turbulent momentum exchange starts to become significant. Simultaneously the velocity gradient is reduced but unlike the accelerated boundary layer at P1 it does not vanish. This leads to a plateau in the loss value of about $\Phi = 1$. At the edge of the displayed wall distance range it finally starts to decrease towards the values of the inviscid core flow. Hence, although the peak loss production is lower at position P4 than at P1, the total loss production is larger due to the velocity gradients in the turbulent part of the boundary layer.

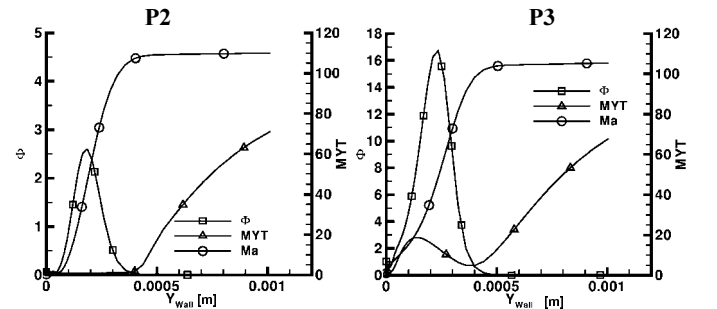


Figure 10: Distribution of Φ , μ_{eff}/μ_t (MYT) and Ma close to the wall in vane 2 (V2_111), mid-span, $Re=300,000$ at position P2 and P3

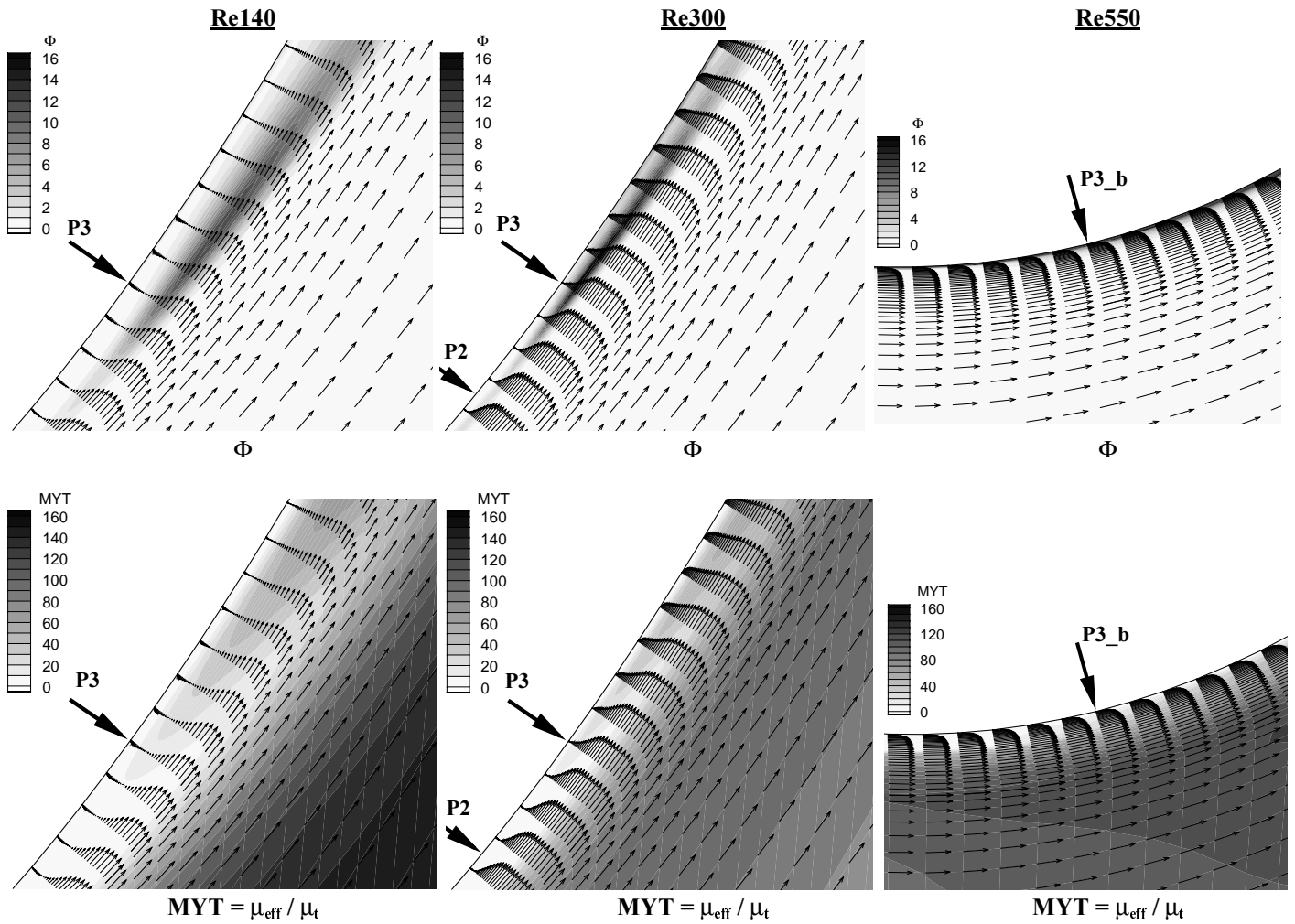


Figure 11: Loss production coefficient Φ and total viscosity in transition region for different Reynolds numbers, vane 2 (V2_111), mid-span

In figure 10 the two cuts through the boundary layer in the proximity of the separation bubble (P2 and P3) are shown. Position P2 is located in the area of the laminar separation bubble upstream of the transition point. The velocity profile shows the typical shape of a separated boundary layer with a concave–convex turning. Close to the wall ($y_{wall} < 0.1$ mm) the flow is separated. There is basically no loss production at the wall due to the absence of any significant velocity gradient. The loss production occurs in the shear layer between the bubble and the free-stream. Its maximum value of approximately 2.5 is relatively low compared to the Φ -values at the wall at P1 and P4. The reason is, that the velocity gradient is not as sharp as in these locations and the flow is still laminar.

The picture changes at position P3, which is located in the transitional region, where turbulence production starts. As can be seen in figure 11, middle picture, the boundary layer has reattached at P3. The velocity profile, however, has still the concave–convex shape. The loss production reaches quite high levels above $\Phi = 15$ at $y_{wall} \approx 0.25$ mm. It is important to note that the loss production at the wall is still close to zero.

The high loss production at location P3 originates from the combination of a significant flow shear layer and the developing

turbulence. Loss production is a direct function of shear and effective viscosity. Here, directly downstream of the separation bubble, the shear layer is located far enough from the wall laminar sublayer to interact with the turbulence production of the transition and thus produces significant loss.

In other words, the presence of the separation bubble detaches the shear layer from the wall. Now the shear layer is completely subject to the developing turbulence downstream of transition onset. The result is a loss tail starting at the outer edge of the separation bubble, peaking in loss production in the transitional region. It eventually fades further downstream due to the smoothing out of the shear layer, which becomes part of the turbulent, decelerating boundary layer. Inside the separation bubble itself basically no loss production occurs, since the velocity gradients inside the bubble are small.

Influence of the Reynolds-Number

As seen above, the presence of a separation bubble on the suction side introduces an additional loss production inside the boundary layer. In figure 11 pictures of the transitional region of the other two Reynolds number cases under investigation are included.

In the $Re = 550,000$ case the transition takes place further upstream than in the other two cases close to position P3_b (fig. 11 and fig. 12). This position is near P1 (fig. 8). The boundary layer flow remains attached to the wall, thus only the shape of the velocity distribution changes from a laminar to a turbulent profile.

At position P3_b transition has already started. Since the boundary layer is not yet decelerated at this position, its thickness is very small, resulting in a steep velocity gradient at the wall. The peak Φ -value at the wall is 75. However, the total loss production is not very large, because the loss coefficient quickly decays with increasing wall distance. Hence, at the high Reynolds number the loss production is mostly concentrated in the region very close to the wall with high loss generation at the wall and little loss generation in the rest of the flow field.

At the lower Reynolds number of 140,000 the same cut-out is taken for the plot in figure 12 as for the Re300 case. The separation bubble is about 4 to 5 times thicker than in the Re300 case. This causes a further shift of the adjacent shear layer away from the wall.

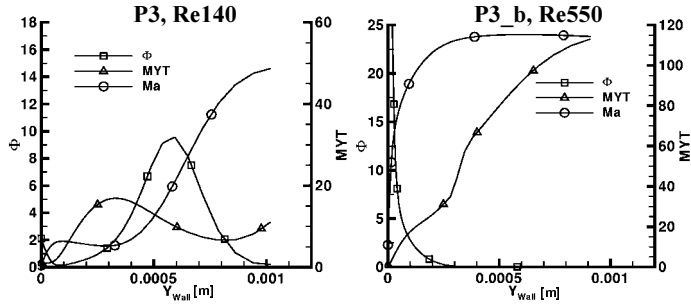


Figure 12: Distribution of Φ , μ_{eff}/μ_t (MYT) and Ma close to the wall in vane 2 (V2_111), mid-span, $Re=140,000$ and $Re = 550,000$

Not only the extend of the bubble normal to the main flow but also its extend in flow direction is considerably larger in the Re140 case than in the Re300 case. The smaller Reynolds number implies also larger relative viscous forces ($Re = \text{ratio of momentum forces to viscous forces}$) in the laminar flow regime. These two aspects lead to the fact that the shear layer in the Re140 case is thicker and thus smoother than in the Re300 case. The result is that the loss production in the shear layer covers a wider range of the flow but with a smaller maximum Φ (fig. 10, 11 and 12).

| | Re140 | Re300 | Re550 |
|--------|-------|-------|-------|
| V2_111 | 2.147 | 1.000 | 1.006 |
| V2_138 | 1.582 | 0.992 | 1.002 |

Table 2: Loss coefficient ζ_v of vane 2 at mid-span, all values referenced to ζ_v of case Re300, V2_111

Effectively, the total loss is considerably higher for the Reynolds number of 140,000 than for the other two Reynolds numbers. As can be seen in table 2 it is more than doubled at mid-span. In the Re140 case the local maximum loss (ζ_v) of the wake is much higher than for the Re300 case (fig. 13). Also, at the low Reynolds-number the suction side flank of the wake widens significantly, indicating a thicker, loss

generating boundary layer, while the onset of the pressure side flank seems to be relatively independent of Reynolds-number effects.

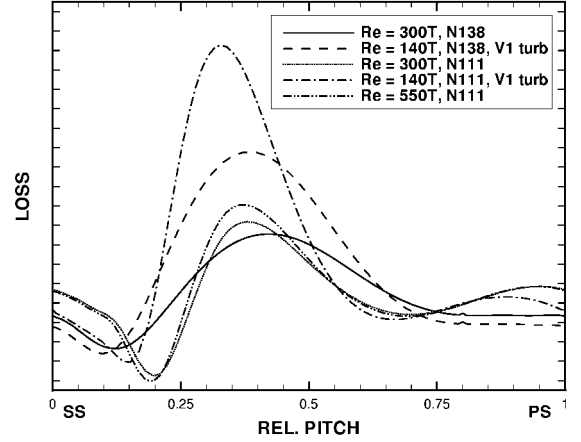


Figure 13: Distribution of ζ_v in circumferential direction at mid-span in plane downstream of vane 2 (20% axial chord downstream of trailing edge)

In figure 14 the suction side boundary layer growth can be clearly seen. While the momentum thickness of the Re140 case is only slightly larger than for the other two Reynolds numbers up to approximately 60 % axial chord length, it grows much faster downstream of the separation bubble at about 70 % axial chord. In the Re140 case the postprocessing stops at 80% axial chord length, where the boundary layer edge reaches the boundary of the numerical O-grid, which covers the airfoil (This is no limitation for the flow solver, only for the postprocessor). But it still can be seen that the momentum thickness there is twice the amount of the higher Reynolds numbers.

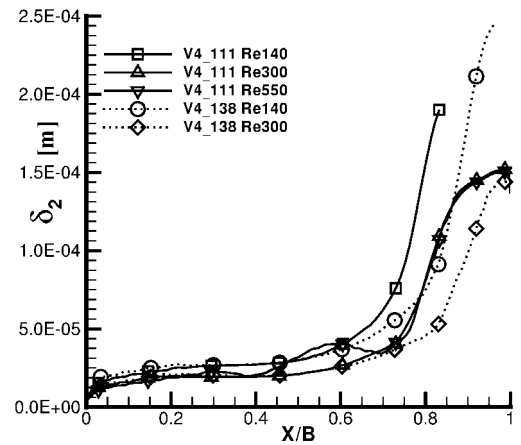


Figure 14: Development of momentum thickness along the suction side boundary layer

Influence of the aerodynamic load

In table 2 the loss of the vane 2 with 138 airfoils is also included. As mentioned above, the two airfoils were designed to perform the same flow turning. Hence, the V2_138 geometry faces a smaller

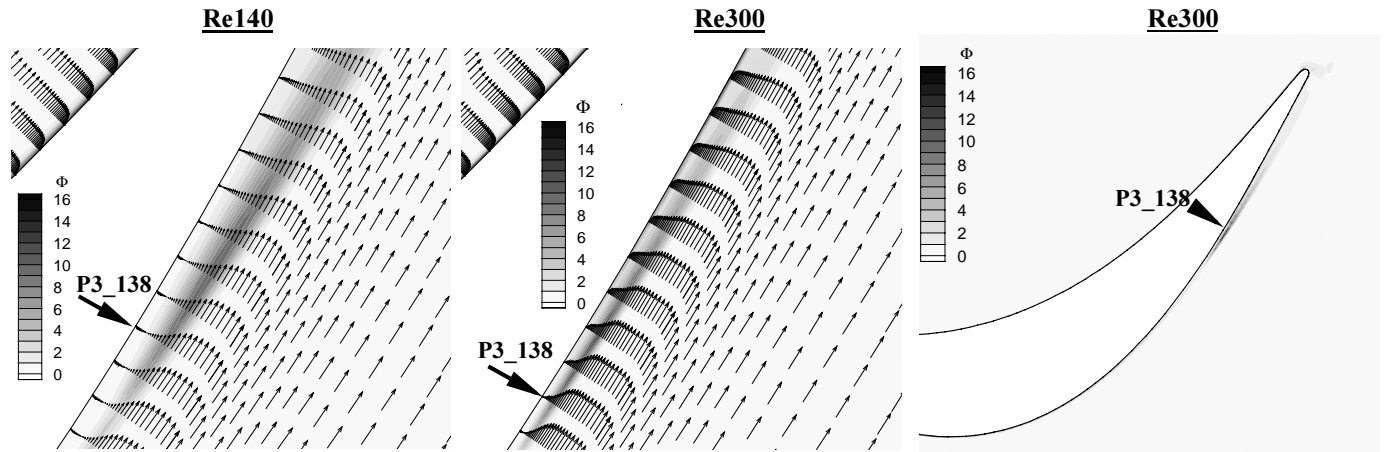


Figure 16: Loss production coefficient Φ in transition region for different Reynolds numbers, vane 2 (V2_138), mid-span

aerodynamic load. This becomes obvious in figure 2, where the two surface pressure distributions are compared.

In terms of the airfoil loss ζ , at mid-span (table 2) an interesting result is to be observed. At the intermediate Reynolds number of 300,000 both configurations exhibit basically the same total pressure loss. There are two opposing influences for these configurations. The higher airfoil load vane (V2_111) produces a slightly higher loss peak in the wake (fig. 13). On the other hand, there are simply more airfoils in the V2_138 configuration with accordingly more surface. Since the relative pitch is displayed in figure 13, the wake of the cases with 138 airfoils appears broader than the wake of the 111 airfoils. Effectively, these two opposing effects compensate each other.

At the low Reynolds number, the loss of the lower airfoil count vane is considerably larger (tab. 2). Especially the peak loss, shown in figure 13 is much higher for that configuration. While at the intermediate Reynolds number (Re300) the maximum loss production Φ is located at 0.2 mm wall distance for both airfoil configurations, it stays closer to the wall for 138 airfoils at the lower Reynolds number, as can be seen by comparing figure 15 with figures 10 and 12. The separation bubble on the vane 2 with 138 airfoils does not grow that much at the lower Reynolds number due to its lower aerodynamic load and different profile design.

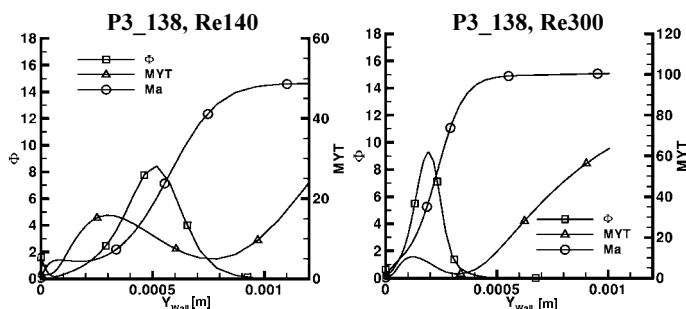


Figure 15: Distribution of Φ , μ_{eff}/μ_t (MYT) and Ma close to the wall in vane 2 (V2_138), mid-span, Re=140,000 and 300,000

As can be seen in figure 16 in comparison to figure 11, The separation bubble in the V2_138 configuration is smaller in its wall-

normal extension and it is located further downstream. As pointed out by Gier et al., 2000 a separation bubble further downstream in a region, where the curvature of the suction side has basically phased out, seems to keep the wake boundary layer thickness and thus the losses small. These differences in boundary layer growth can again be obtained from figure 14. At both Reynolds numbers the momentum thickness is quite similar for the respective airfoil configurations. But in the region of the separation bubble the boundary layer thicknesses of the V2_111 cases and especially of the V2_111 at Re = 140,000 eventually grow stronger. This corresponds to the impact of the steeper positive pressure gradient on the rear part suction side of the V2_111 airfoil (fig.2).

The resulting higher profile loss of the lower airfoil count configuration is compensated by the smaller total surface of the 111 airfoils in the 2nd guide vane row at Re = 300,000. At the low Reynolds number the profile loss increase of the 111-airfoil configuration, however, strongly exceeds the profile loss increase of the 138-airfoil configuration.

Summarising, it has to be noted that within the investigated Reynolds number range, although both airfoil configurations provide the necessary turning of the flow without a full flow separation, there seem to be different optimal airfoil numbers per grid row at different Reynolds numbers as far as loss reduction is concerned. This behaviour should be taken into account for the design of aero engines with respect to their size and mission profile.

CONCLUSIONS

In this paper the flow in a three-stage LP turbine, which is typical for jet engine design has been investigated in detail by the use of a modern 3D Navier-Stokes solver. The numerical investigations were complemented by experimental data gathered in the test turbine.

In order to assess the flow structure details and overall performance information with a high degree of quality, a reliable transition model was successfully combined with the $k-\omega$ turbulence model. The simulations corresponded well with the experimental data. The investigation focussed on the loss generation mechanisms in the core flow around mid-span.

By analysing the flow structure and loss production it was shown that the loss generation inside the suction side separation bubble, which was present at the two lower Reynolds-numbers, is neglectable. The significant loss increase at low Reynolds numbers is caused by the fact that the separation bubble shifts the shear layer away from the wall and thus makes it subject to the developing turbulence at laminar – turbulent transition. The additional loss production occurring in this shear layer is responsible for the possibly significant loss increase with decreasing Reynolds numbers.

This additional loss generation is a function of the flow structure and thus of the airfoil shape and pressure distribution. By comparing two airfoils in the second guide vane with 111 and 138 airfoils, respectively, this could be investigated. While the profile loss was similar at the intermediate (design) Reynolds number, the performance of vane 2 with the higher aerodynamic load decreased significantly faster with further Reynolds number reduction.

It was found that this happens, because the additional loss generation in the wall detached shear layer increases much more at the low Reynolds-number for high aerodynamic loads (low airfoil count configuration). At the intermediate (design) Reynolds number the somewhat larger profile loss of this configuration is compensated by its smaller total airfoil surface.

These implications should be taken into account in the design of aircraft engines, operating at conditions, where laminar flow separation, reattachment and transition can occur. In this case the engine size and the flight mission should have an impact on the airfoil design, as turbine efficiency is an important issue for operating cost.

ACKNOWLEDGEMENT

The support for code development and validation as well as experimental and numerical investigation of the turbine rig through the German *Ministry of Education and Research* under the *E3E* program is gratefully acknowledged.

The numerical code TRACE used in this investigation was jointly developed by *MTU Aero Engines* and the *Institute for Propulsion Technology* of the *German Aerospace Research Establishment (DLR)*.

REFERENCES

- Abu-Ghannam, B.J., Shaw, R., 1980, "Natural Transition of Boundary Layers – The Effects of Turbulence, Pressure Gradient and Flow History", *J. of Mechanical Engineering Science*, Vol. 22, No. 5, pp. 213 – 228
- Baldwin, B., Lomax, H., 1978, "Thin Layer Approximation and Algebraic Model for Separated Turbulent Flows", *AIAA Paper 78-257*
- Denton, J.D., 1993, "Loss Mechanisms in Turbomachines", *ASME Paper 93-GT-435*
- Drela, M., 1995, "Implementation of Modified Abu-Ghannam/Shaw Transition Criterion", *MIT Aero-Astro*
- Dorney, D.J., Ashpis, D.E., Halstead, D.E., Wilser, D.C., 1999, "Study of Boundary Layer Development in a Two-Stage Low-Pressure Turbine", *AIAA Paper 99-0742*
- Chernobrovkin, A., Lakshminarayana, B., 1999, "Turbulence Modeling and Computation of Viscous Transitional Flows for Low

Pressure Turbines", *ASME J. of Turbomachinery*, Vol.121, pp. 824 – 833

Engber, M., Fottner, L., 1995, The Effect of Incoming Wakes on Boundary Layer Transition of a Highly Loaded Turbine Cascade, AGARD PEP 85th Symposium on "Loss Mechanisms and Unsteady Flows in Turbomachines", Derby, UK, 8-12 May 1995

Fritsch, G., Hoeger, M., Blaha, C., Bauer, D., 1997, "Viscous 3D Compressor Simulations on Parallel Architectures", *AIAA Paper 97-2876*

Gier, J., Ardey, S., Heisler, A., 2000, "Analysis of Complex Three-Dimensional Flow in a Three-Stage LP Turbine by means of Transitional Navier-Stokes Simulation", *ASME Paper 2000-GT-645*

Hatman, A., Wang, T., 1998a, "Separated-Flow Transition Part 2 – Experimental Results", *ASME-Paper 98-GT-462*

Hatman, A., Wang, T., 1998b, "A Prediction Model for Separated-Flow Transition", *ASME-Paper 98-GT-237*

Mayle, R.E., 1991, "The role of Laminar-Turbulent Transition in Gas Turbine Engines", *ASME J. of Turbomachinery*, Vol.113, pp. 509 – 537

Mayle, R.E., Schulz, A., 1996, "The Path to Predicting Bypass Transition", *ASME J. of Turbomachinery*, Vol.119, pp. 405 – 411

Rivir, R.B., 1996, "Transition on Turbine Blades and Cascades at Low Reynolds Numbers", *AIAA Paper 96-2079*

Roberts, W.B., 1980, "Calculation of Laminar Separation Bubbles and Their Effect on Airfoil Performance", *AIAA Journal*, Vol. 18, No. 1, pp. 25 – 31

Sanz, W., Platzer, M.F., 1996, "On the Navier-Stokes Calculation of Laminar Separation Bubbles using Different Transition Models", *ASME Paper 97-GT-453*

Schröder, T., 1991, "Investigation of Blade Row Interaction and Boundary Layer Transition Phenomena in a Multistage Aero Engine Low-Pressure Turbine by Measurements with Hot-Film Probes and Surface-Mounted Hot-Film Gauges", *VKI Lecture Series 1991-06*, Boundary Layers in Turbomachines

Scrivener, C.T.J., Connolly, C.F., Cox, J.C., 1991, "Use of CFD in the Design of a Modern Multistage Aero Engine LP Turbine Design", *Paper IMechE Conference C423/056*

Sohn, K.H., Shyne, R.J., DeWitt, K.J., 1998, "Experimental Investigation of Boundary Layer Behavior in a Simulated Low Pressure Turbine", *ASME Paper 98-GT-34*

Stratford, B.S., 1957, "Flow in the Laminar Boundary Layer near Separation", *Reports and Memoranda No. 3002*, Nov. 1954

Swanson, R.C., Turkel, E., 1987, "Artificial Dissipation and Central Difference Schemes for the Euler and Navier-Stokes Equations", *AIAA Paper 87-1107*

Tan, A.C.N., Auld, D.J., 1991, "Experimental Investigations of Laminar to Turbulent Boundary Layer Transition with Separation Bubbles at Low Reynolds Numbers", *Proceedings Boundary Layer Transition and Control*, Cambridge, UK, 8.-12. April 1991

Qiu, S., Simon, W., 1997, "An Experimental Investigation of Transition as Applied to Low Pressure Turbine Suction Surface Flows", *ASME Paper 97-GT-455*

Walker, G.J., Subroto, P.H., Platzer, M.F., 1988, "Transition Modelling Effects on Viscous/Inviscid Interaction Analysis of Low Reynolds Number Airfoil Flows Involving Laminar Separation Bubbles", *ASME Paper 88-GT-32*

Wilcox, D.C., 1988, "Reassessment of the Scale Determining Equation for Advanced Turbulence Models", *AIAA Journal*, Vol. 25, No. 11, pp. 1299 - 1310